Supporting Information

Spin-crossover in an organic-inorganic hybrid perovskite

Wei-Wei Wu,[a] Si-Guo Wu,[a] Yan-Cong Chen,[a] Guo-Zhang Huang,[a] Bang-Heng Lyu,[a] Zhao-Ping Ni*[a] and Ming-Liang Tong*[a]

Table of Contents

Experimental Details

Table S1. Crystallographic data for **1**.

Table S2. Selected structural parameters for **1** at different temperatures.

Table S3. The structural parameters of C-H···π interactions in **1** at different temperatures.

Table S4. The structural parameters of π···π interactions in **1** at different temperatures.

Figure S1. PXRD pattern of **1**.

Figure S2. TG curve of **1**.

Figure S3. Asymmetric unit of **1** at 120 K.

Figure S4. The 3D anionic framework of **1**.

Figure S5. The Intermolecular interactions of **1**.

Figure S6. The 1st derivative of magnetic data.

Figure S7. Two consecutive thermal cycles of magnetic measurements at sweep rate of 2 K min^{-1}.

Figure S8. Variable-temperature magnetic susceptibility and the 1st derivative of magnetic data at different sweep rates for **1**.

Figure S9. Variable-temperature magnetic susceptibility and the 1st derivative of magnetic data in settle mode for **1**.

Figure S10. Differential scanning calorimetry (DSC) curves at 10 K min^{-1} for **1**.

Figure S11. The 1st derivative of photomagnetic data.

Figure S12. Temperature-dependent fluorescence emission spectra of PPNCl and **1**.

Figure S13. The first derivative plot of normalized fluorescence emission intensity at 438 nm as a function of temperature for **1**.

Figure S14. Normalized fluorescence emission intensity at 438 nm as a function of temperature for **1**. The intensity at low temperature region is linearly fitted to extract the base line of thermal fluorescence quenching.

Figure S15. The UV/Vis reflectivity spectroscopy of PPNCl and **1** at room temperature.

Experimental Details

General Procedure.

The FT-IR spectra were recorded in KBr tablets in the range of 4000−400 cm^{-1} on Thermo Nicolet 6700-Contiuμm FT-IR spectrometer. The powder XRD patterns were recorded on a Rigaku Smartlab X-Ray diffractometer with Cu$_{K\alpha}$ (λ = 1.54178 Å) radiation. Thermogravimetric analyses (TG) were recorded on TG209 F1 Libra. The C, H, and N microanalyses were performed on an Elementar Vario-EL CHNS elemental analyzer. Differential Scanning Calorimetry (DSC) measurement was performed by cooling and heating the crystals in an aluminium crucible using a NETZSCH5, which was carried out at sweeping rate of 10 K min^{-1} under nitrogen. The surface reflectivity measurements were performed in the range of 200–800 nm on a SHIMAZU UV-3600Plus UV-ViS-NIR Spectrophotometer equiped with an integrating sphere. Iodine-tungsten lamp and xenon lamp were used as the spectroscopic lights. The measurements were calibrated by baryum sulfate as the reference sample. Fluorescence emission spectra were recorded on the solid samples on an Edinburgh FL 980 fluorescence spectrophotometer equipped with Xenon light and coupled with the ARS cryostat.

Synthesis

All the chemical reagents were commercially available and used as received. (PPN)[Fe{Au(CN)$_2$}$_3$] (**1**) was prepared by the slow diffusion technique. The solutions of Fe(ClO$_4$)$_2$·6H$_2$O (0.025 mmol, 6 mg) in EtOH (0.5 mL) and (PPN)[Au(CN)$_2$] (0.075 mmol, 59 mg) in EtOH (2 mL) were placed in a test tube in the upper and lower layers, respectively. The middle layer was filled with 5 mL EtOH. The pale yellow block crystals were collected after two weeks. Yield: 45%. Anal. Calcd for $C_{42}H_{30}Au_3FeN_7P_2$: C, 37.61; H, 2.25; N, 7.31. Found: C, 37.60; H, 2.16; N, 7.41. IR (KBr, cm^{-1}): 2177 (vs, C≡N).

Magnetic measurements

Magnetic susceptibility measurements at different sweep rates (0.5, 1, 2, 4 K min^{-1}) were performed on a Quantum Design PPMS magnetometer operating under a field of 5000 Oe. Magnetic susceptibility measurement in settle mode (with no overshoot mode) was also performed, in which 0.5 and 5 K steps were set in the ranges of 300−120 K and 120−10 K, respectively. The actual "averaged" cooling/warming rates in the range of 300−120 K are 0.14 and 0.12 K min^{-1}, respectively. Diamagnetic correction was performed based on Pascal's constants. Photomagnetic behaviors were studied on a Quantum Design MPMS XL-7 SQUID magnetometer operating under a field of 1 T. The crystalline sample (~2.5 mg) was introduced into the standard fiber optic sample holder (FOSH). The exact sample mass was corrected by the variable-temperature magnetic susceptibility data measured on a larger amount of sample. The sample was first slowly cooled to 10 K, and irradiated by a 473 nm laser (~20 mW/cm^2) until photo-saturation and then turned off the light. The temperature increased to 100 K in the dark and the magnetization measured every 1 K in settle mode to determine the *T*(LIESST) value.

X-ray Crystallography

Single-crystal diffraction data were recorded on a Bruker D8 QUEST diffractometer with Mo$_{K\alpha}$ (λ = 0.71073 Å) radiation in sequence at 298, 191, 162 and 120 K for **1**. All non-hydrogen atoms were refined anisotropically by least-squares on F2 using the SHELXTL 2014/7 program.[1] Hydrogen atoms on organic ligands were generated by the riding mode. CCDC 1977206(298 K), 1977205(191 K), 1977204(162 K) and 1977203(120 K) contain the supplementary crystallographic data for this paper. These data could be obtained free of charge from the Cambridge Crystallographic Data Centre via www.ccdc.cam.ac.uk/data_request/cif.

Reference

1 (*a*) Sheldrick, G. M.SHELXS-97, Program for Crystal Structuresolution.University of Göttingen, Germany **1997**. (*b*) Sheldrick, G. M.SHELXL-97, Program for Crystal Structure Refinement. University of Göttingen, Germany **1997**. (*c*) Sheldrick,G.M. Crystal structure refinement with SHELXL. *Acta Crystallogr. C* **2015**, *71*, 3–8.

Table S1. Crystallographic data for **1**.

Parameter	**298 K**	**191 K**	**162 K**	**120 K**
chemical formula	$C_{42}H_{30}Au_3FeN_7P_2$	$C_{42}H_{30}Au_3FeN_7P_2$	$C_{42}H_{30}Au_3FeN_7P_2$	$C_{42}H_{30}Au_3FeN_7P_2$
Mr	1341.42	1341.42	1341.42	1341.42
crystal system	trigonal	trigonal	trigonal	trigonal
space group	$R\bar{3}c$	$R\bar{3}c$	$R\bar{3}c$	$R\bar{3}c$
a/Å	15.5023(7)	15.2390(9)	15.0857(8)	14.9822(5)
b/Å	15.5023(7)	15.2390(9)	15.0857(8)	14.9822(5)
c/Å	31.5971(12)	31.3855(15)	31.2708(14)	31.1973(10)
α/°	90	90	90	90
β/°	90	90	90	90
γ/°	120	120	120	120
V/Å	6576.1(6)	6312.1(8)	6163.2(7)	6064.6(4)
Z	6	6	6	6
μ(Mo Kα)/mm^{-1}	10.442	10.879	11.142	11.323
reflns collected	51693	49891	48041	56341
indep reflns	1832	1825	1703	1566
R_{int}	0.0850	0.0842	0.0871	0.0460
$R_1{}^a(I > 2\sigma(I))$	0.0446	0.0430	0.0250	0.0193
$wR_2{}^b$ (all data)	0.1235	0.1031	0.0590	0.0457
GOF	1.090	1.230	1.069	1.082
largest diff. peak/hole	1.98/-3.54	1.19/-4.12	1.08/-1.78	1.47/-4.61

$^aR_1 = \Sigma|F_o| - |F_c||/\Sigma|F_o|$; $^bwR_2 = \{[\Sigma w(F_o{}^2 - F_c{}^2)^2]/\Sigma[w(F_o{}^2)^2]\}^{1/2}$.

Table S2. Selected structural parameters for **1** at different temperatures.

Parameter	**298 K**	**191 K**	**162 K**	**120 K**
<Fe–N>[a]	2.144(6)	2.025(6)	1.976(3)	1.939(2)
<Au–C>[a]	1.978(7)	1.997(8)	1.990(4)	1.986(3)
<C–N>[a]	1.122(5)	1.130(10)	1.134(5)	1.141(4)
<Fe···Au>[a]	5.2191(4)	5.1348(4)	5.0879(3)	5.0563(3)
ΣFe[b]	16.8(3)	16.8(2)	15.46(12)	13.55(10)
Fe–N–C[b]	169.7(7)	173.2(6)	174.4(3)	175.0(2)
C–Au–C[b]	177.4(5)	177.7(4)	177.2(2)	177.69(16)

[a]The unit of bond length is Å; [b]The unit of angle is °.

Table S3. The structural parameters of C−H···π interactions in **1** at different temperatures.

Parameter	**298 K**	**191 K**	**162 K**	**120 K**
< H4···C1>[a]	2.869(11)	2.790(10)	2.785(5)	2.754(1)
< H7···C1>[a]	2.986(8)	2.922(7)	2.902(4)	2.875(3)

[a]The distance between the hydrogen atom of phenyl group and the carbon atom of cyanide groups in **1**.

Table S4. The structural parameters of π···π interactions[a] in **1** at different temperatures.

Parameter	**298 K**	**191 K**	**162 K**	**120 K**
Θ^{b} (Å)	0	0	0	0
Z^{c} (Å)	4.8182(2)	4.5857(3)	4.4741(3)	4.3732(2)
d^{d} (Å)	3.6666	3.5786	3.5308	3.49
r^{e} (Å)	3.126	2.86745	2.7479	2.635

[a]C2-C7 (2/3+x-y, 4/3-y, 5/6-z; and -1/3-x+y, 1/3+y, -1/6+z); [b]The dihedral angle between two aromatic rings (°); [c]The distance between the centroids of aromatic rings (Å); [d]The perpendicular distance between two aromatic rings (Å); [e]The offset distance between two aromatic rings (Å).

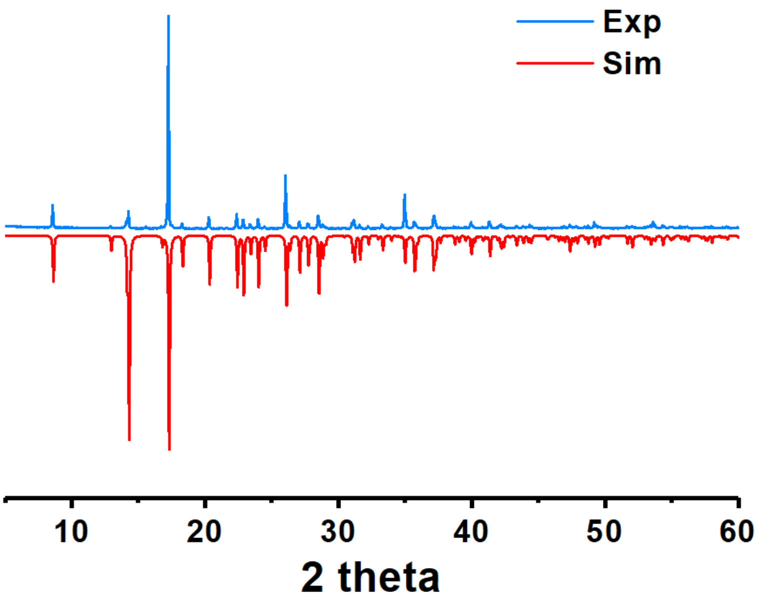

Figure S1. Powder X-ray diffraction data of **1** at room temperature.

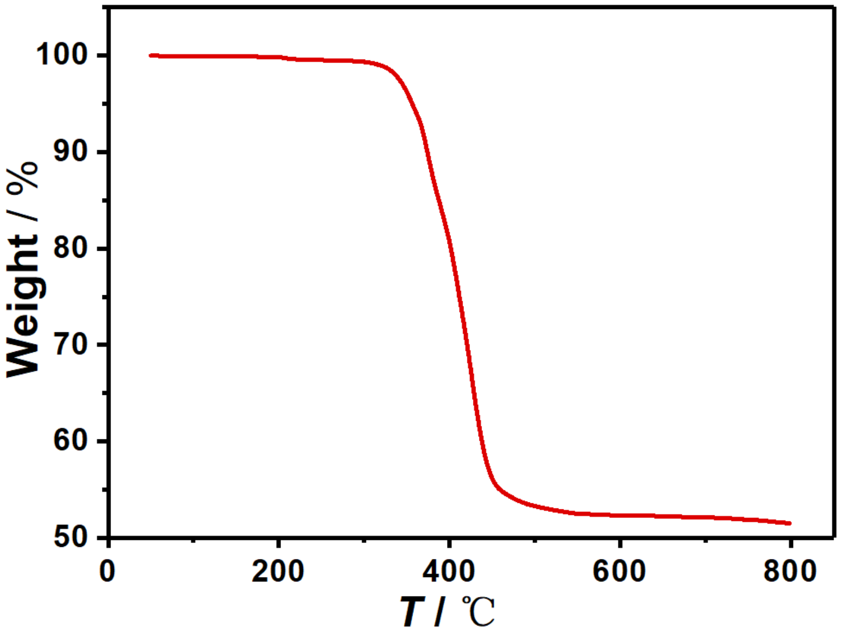

Figure S2. Thermogravimetric analyses of **1** in the N_2 atmosphere with a heating rate of 10 °C min^{-1}.

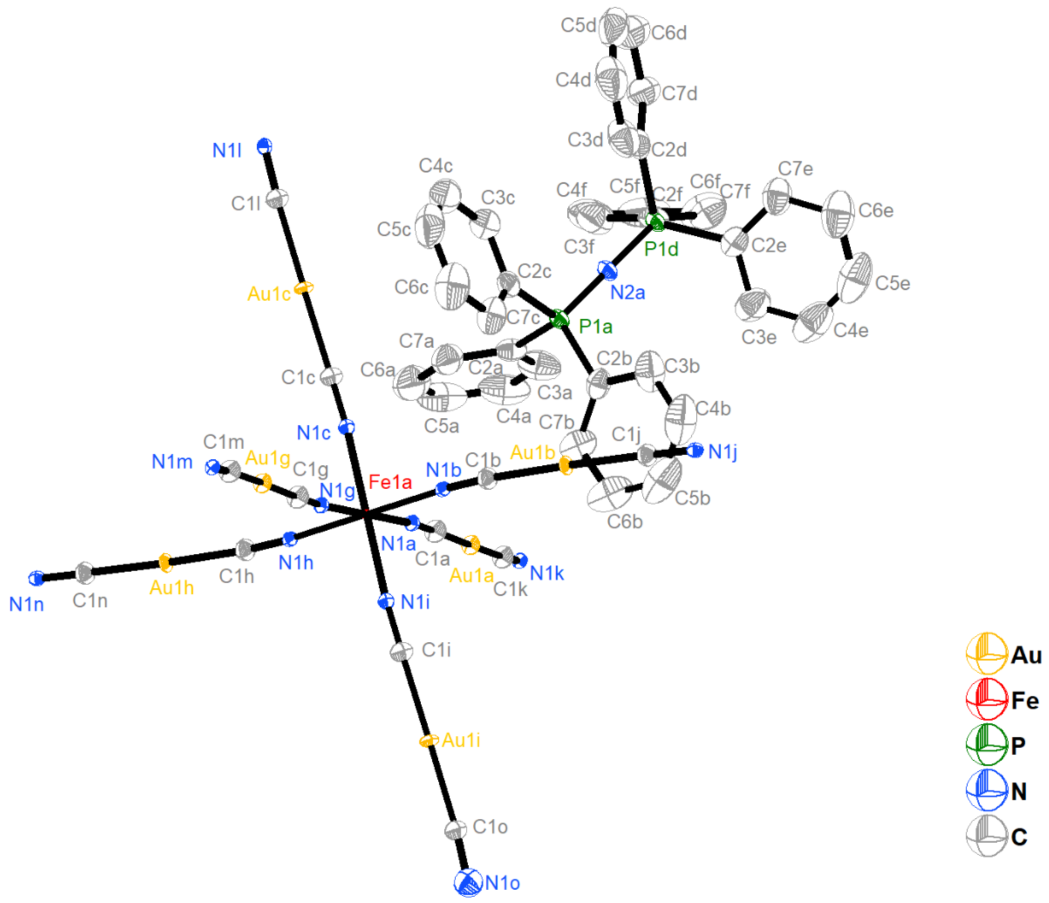

[a]x, y, z; [b]1-y, 1+x-y, z; [c]-x+y, 1-x, z; [d]2/3-x, 4/3-y, 5/6-z; [e]2/3-x, 1/3-X+y, 5/6-z; [f]-1/3+y, 1/3+x, 5/6-z; [g]2/3-x, 4/3-y, 4/3-z; [h]-1/3+y, 1/3-x+y, 4/3-z; [i]2/3+x-y, 1/3+x, 4/3-z; [j]1/3+y, 2/3+x, 7/6-z; [k]1/3+x-y, 2/3-y, 7/6-z; [l]1/3-x, 2/3-x+y, 7/6-z; [m]1/3-x+y, 2/3+y, 1/6+z; [n]1/3-y, 2/3-x, 1/6+z; [o]1/3+x, 2/3+x-y, 1/6+z

Figure S3. Asymmetric unit of **1** at 120 K. Thermal ellipsoids are drawn at the 30% probability. Hydrogen atoms are omitted for clarity.

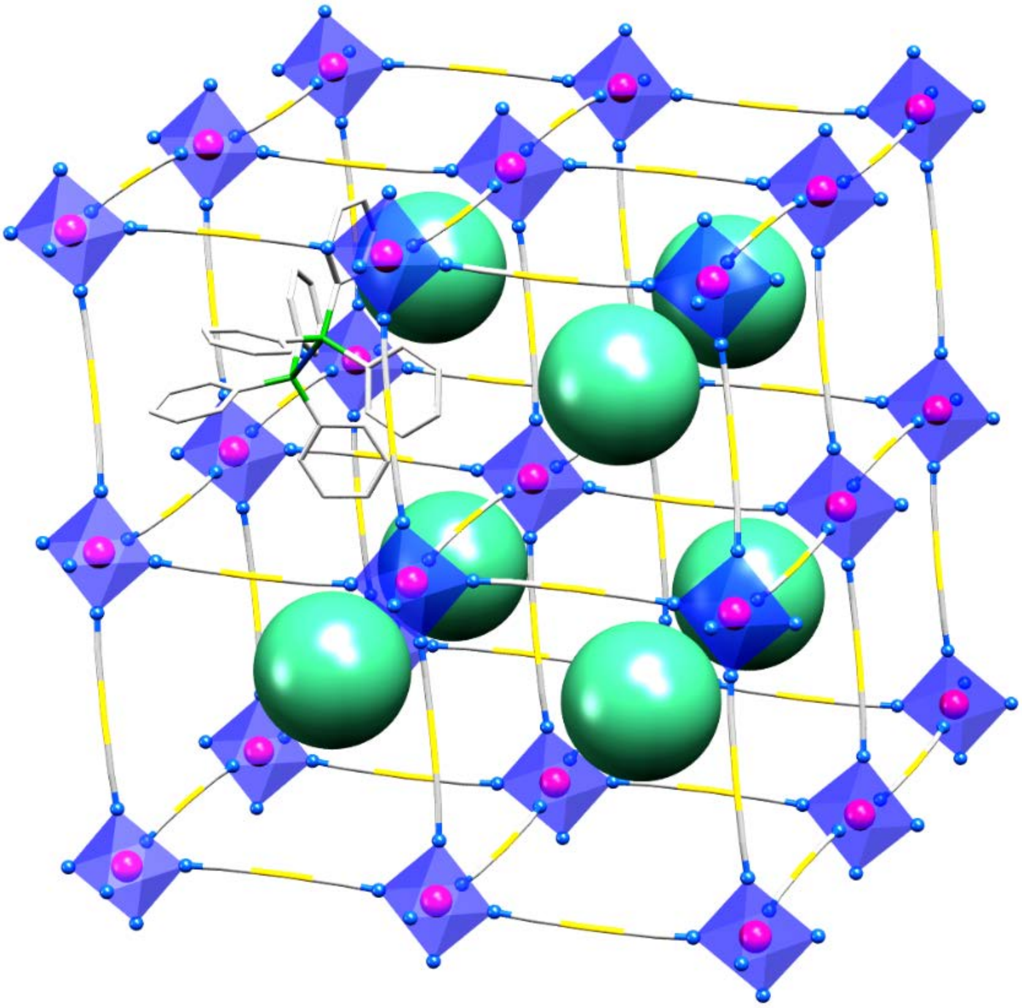

Figure S4. The 3D anionic framework of **1**. Color code: gray (C), blue (N), green (P), red (Fe), yellow (Au), violet (polyhedron), and light green ball (PPN^+).

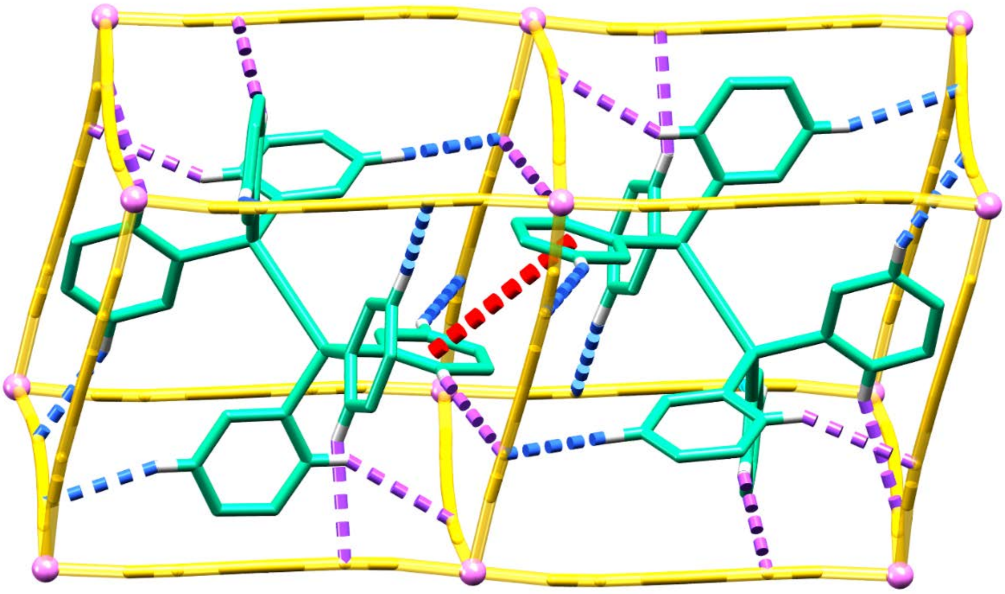

Figure S5. The Intermolecular interactions of **1**: offset π···π interactions between two phenyl groups from neighbouring cubes (red dashed line), C4-H4···π interactions (blue dashed lines) and C7-H7···π interactions (purple dashed lines). Color code: pink (Fe), white (hydrogen), blue green (PPN^+) and golden ($[Au(CN)_2]^-$). Only the hydrogen atoms on C4 and C7 are shown.

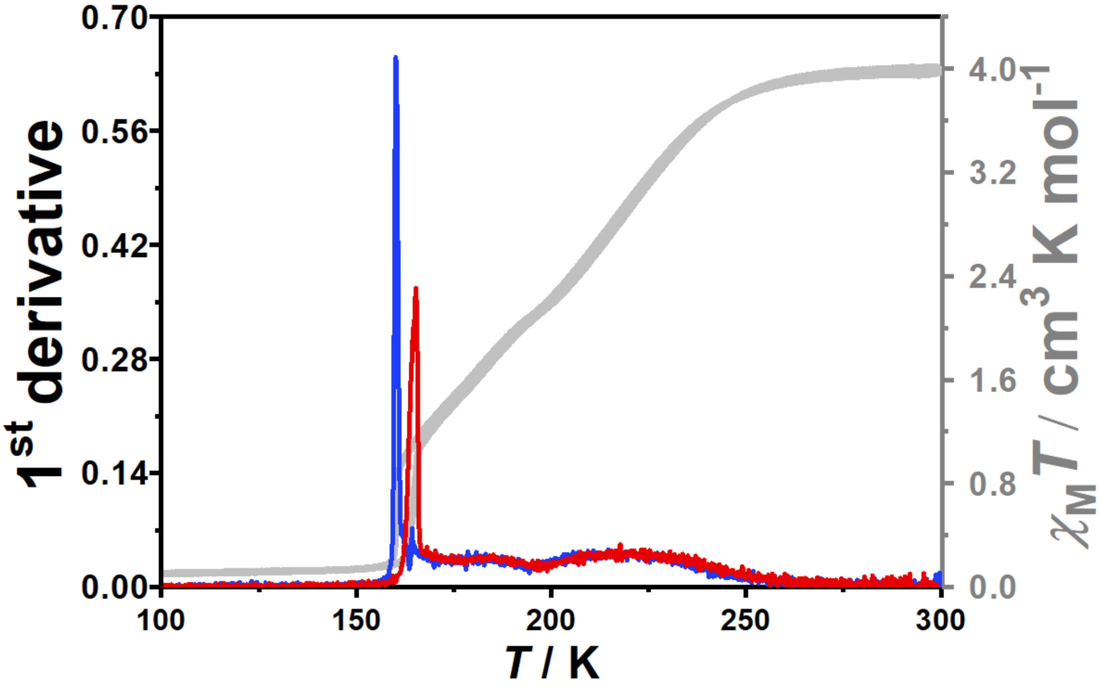

Figure S6. The 1st derivative of magnetic susceptibility data.

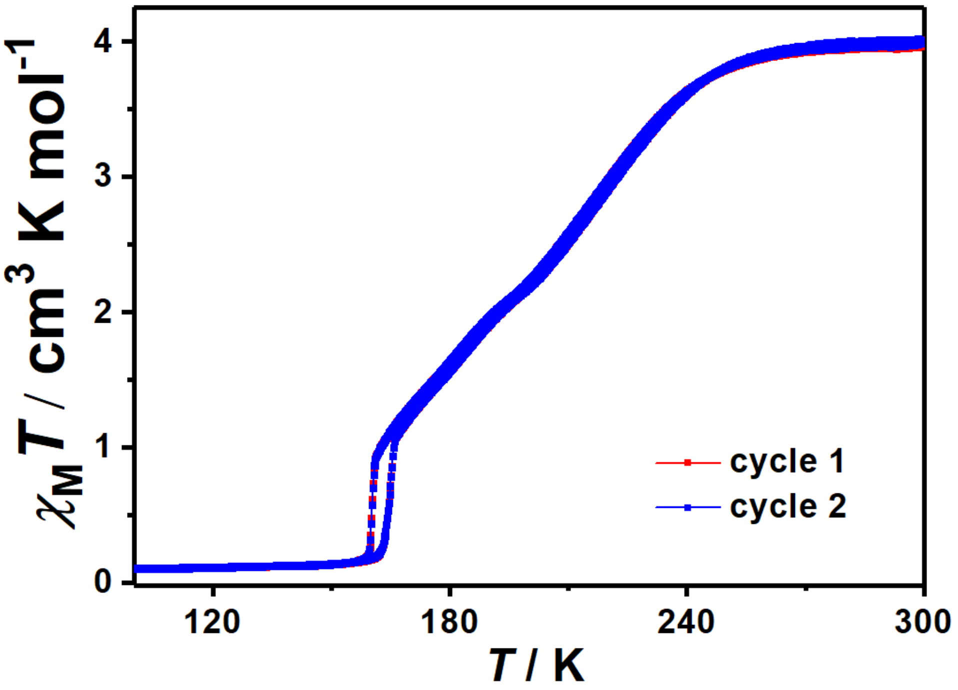

Figure S7. Two consecutive thermal cycles of magnetic measurements at sweep rate of 2 K min^{-1}

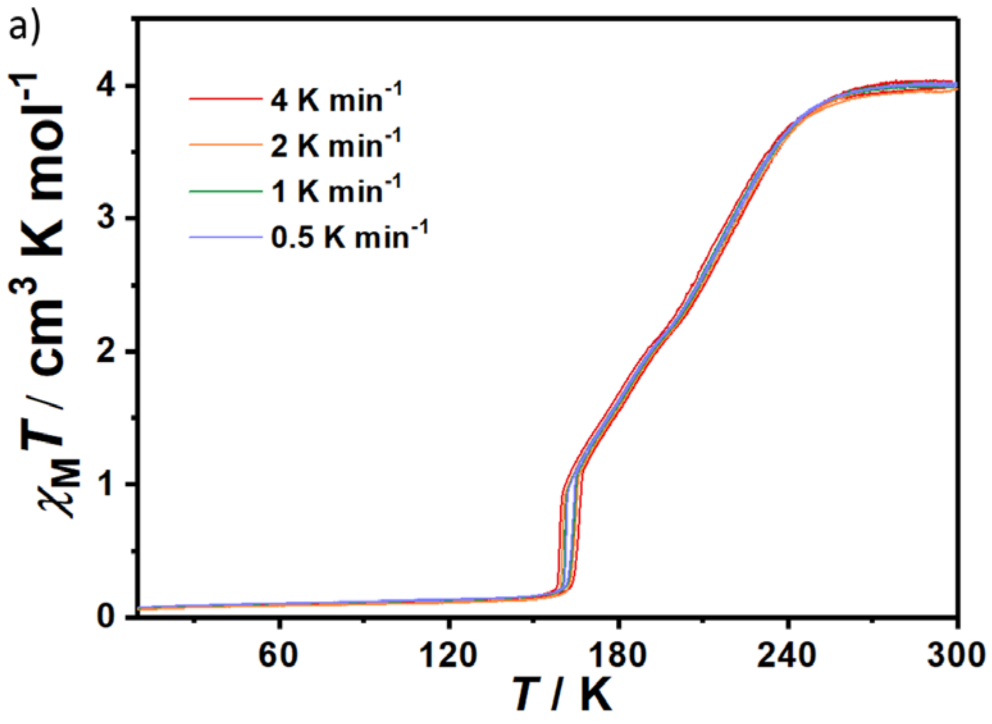

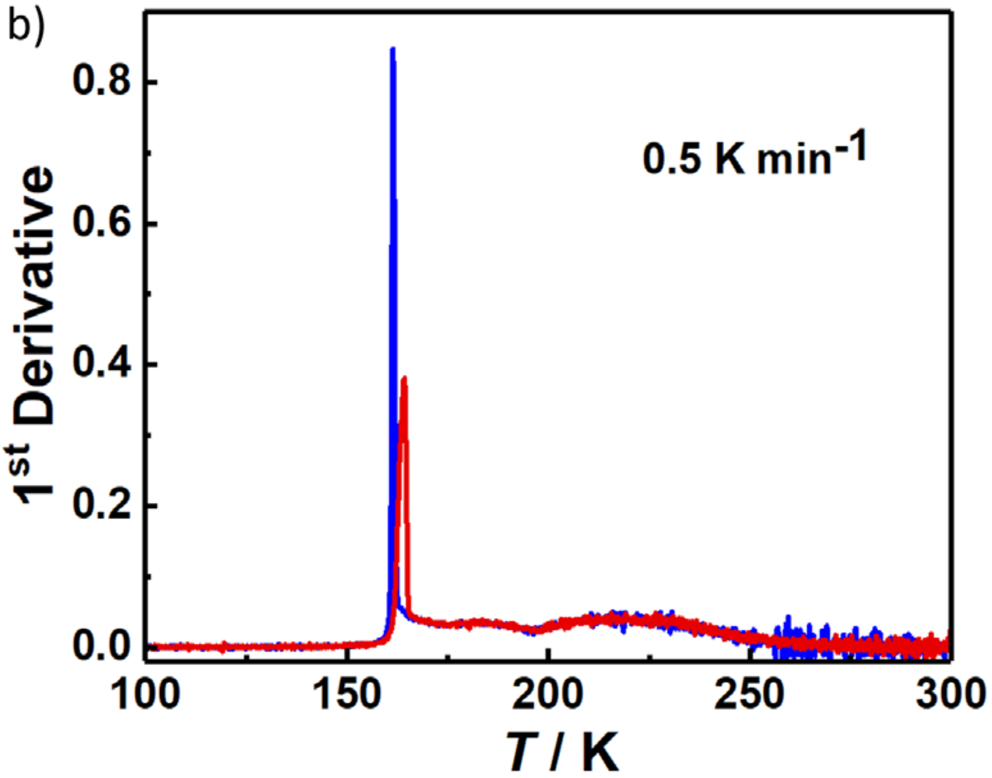
b)
0.5 K min^{-1}
1st Derivative
0.0
0.2
0.4
0.6
0.8
100
150
200
250
300
T / K

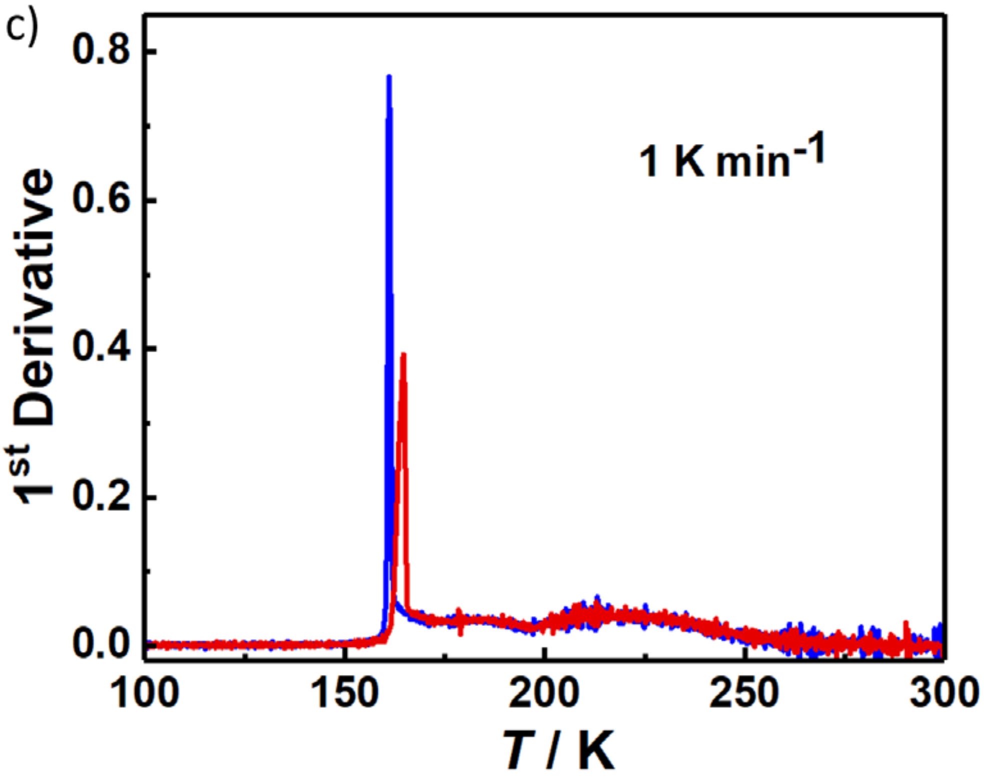
c)
1 K min^{-1}
1st Derivative
0.0
0.2
0.4
0.6
0.8
100
150
200
250
300
T / K

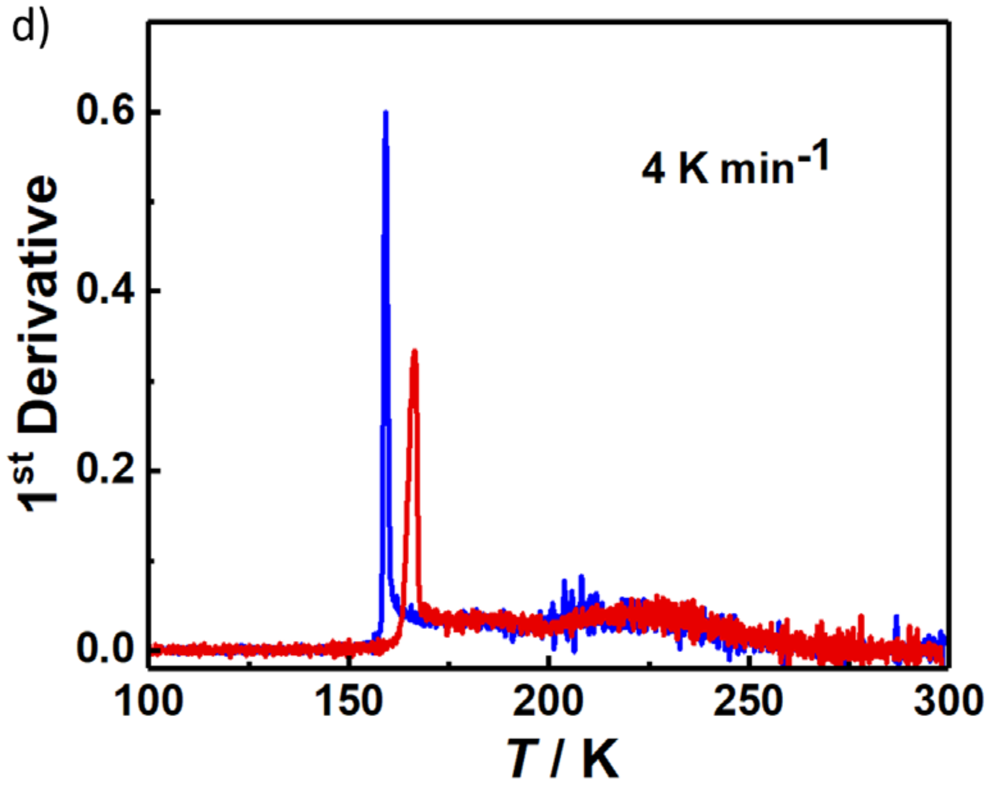

Figure S8. Variable-temperature magnetic susceptibility data at different sweep rates (0.5, 1, 2 and 4 K min^{-1}) for **1** (a). The 1st derivative of magnetic susceptibility data at different sweep rates (0.5, 1 and 4 K min^{-1}) for **1** (b, c, d).

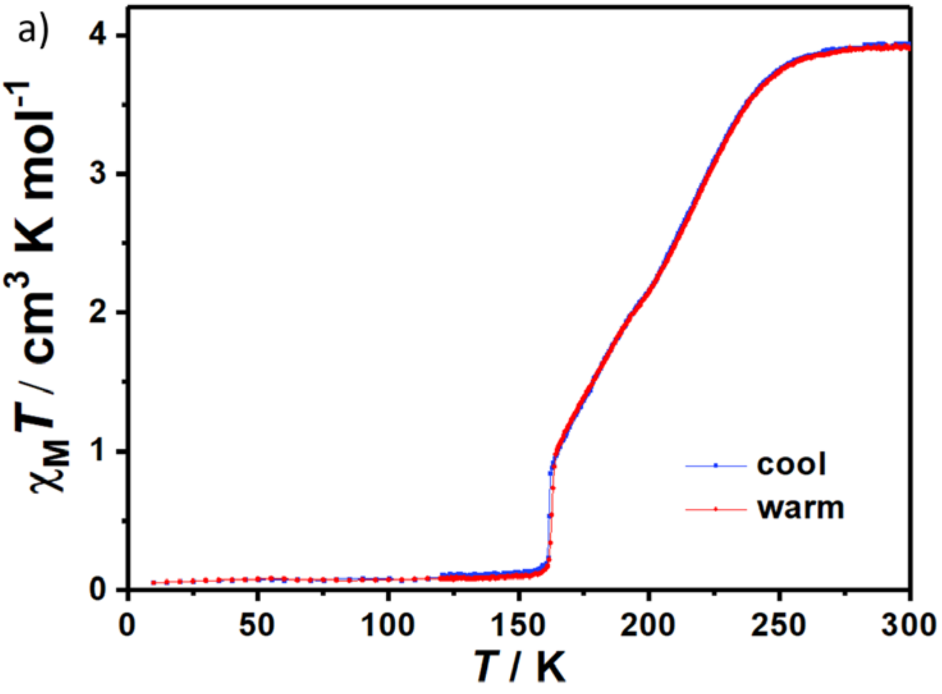

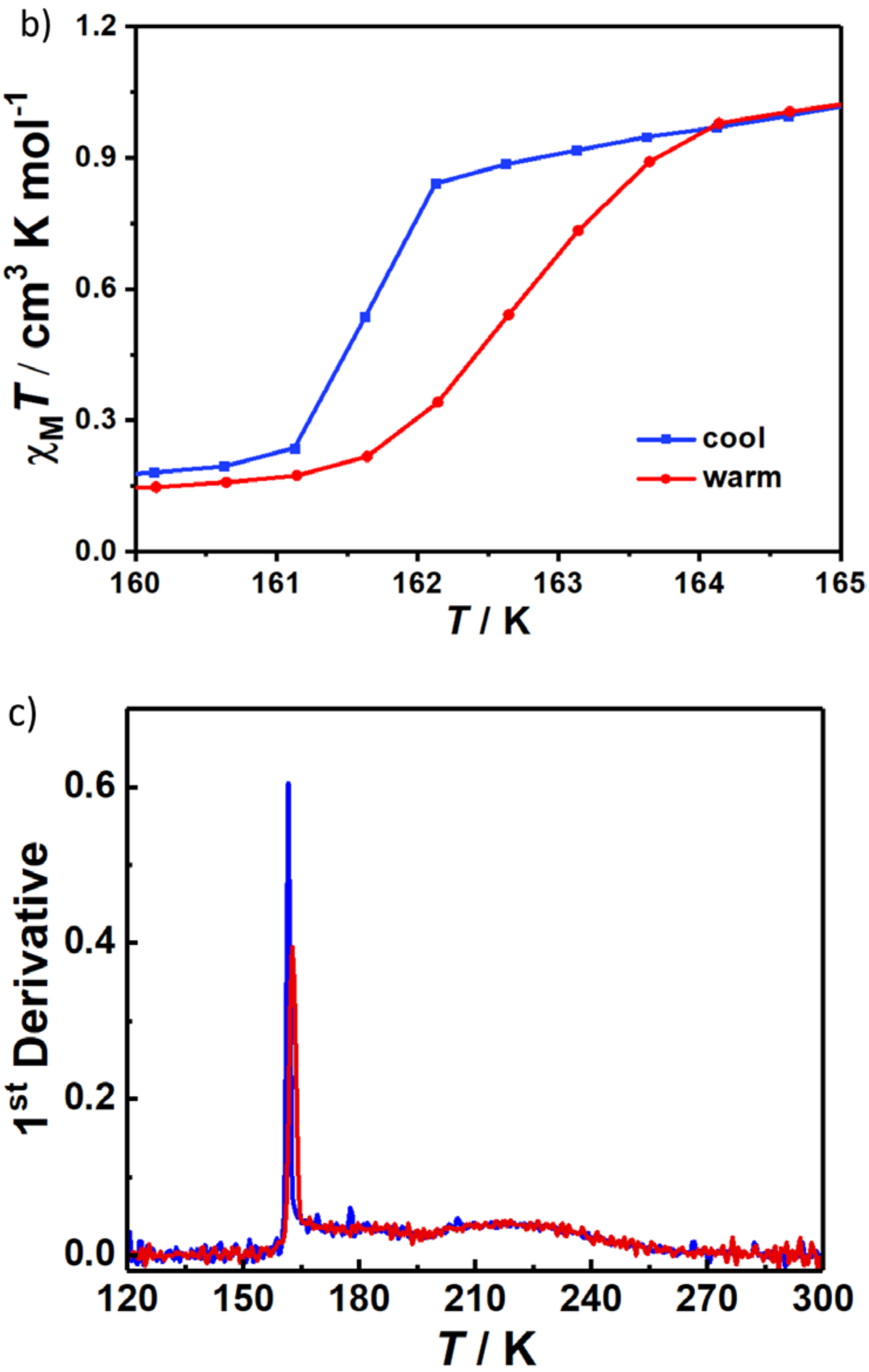

Figure S9. Variable-temperature magnetic susceptibility in settle mode (a). The hysteresis loop is enlarged in (b). The 1st derivative of magnetic susceptibility data in settle mode for **1** (c).

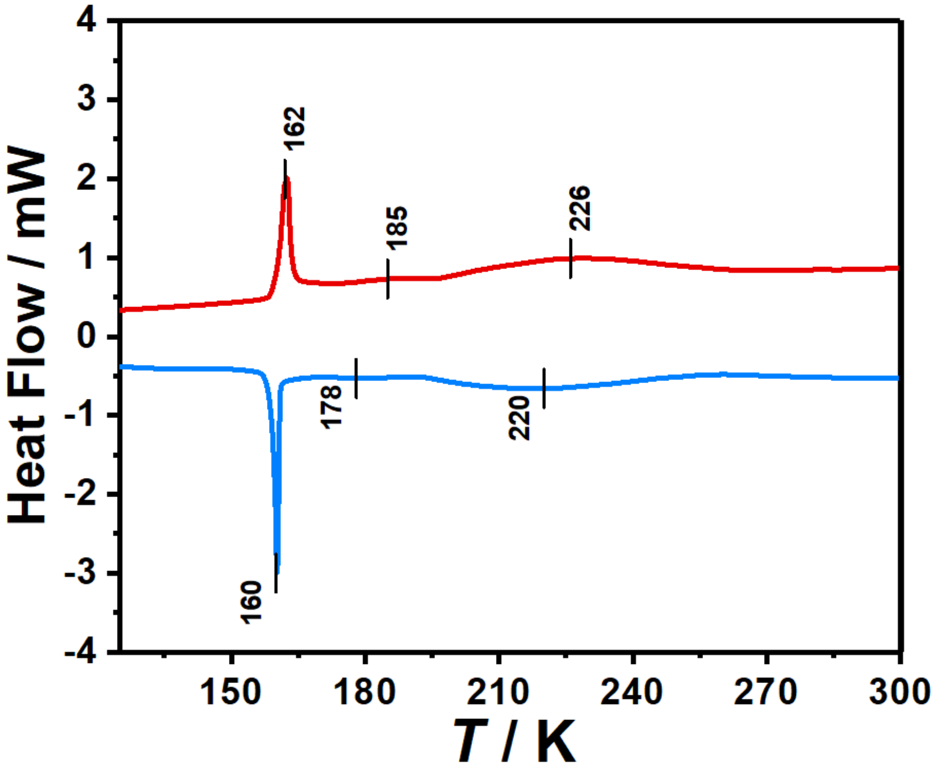

Figure S10. Differential scanning calorimetry (DSC) curves at 10 K min^{-1} for **1**.

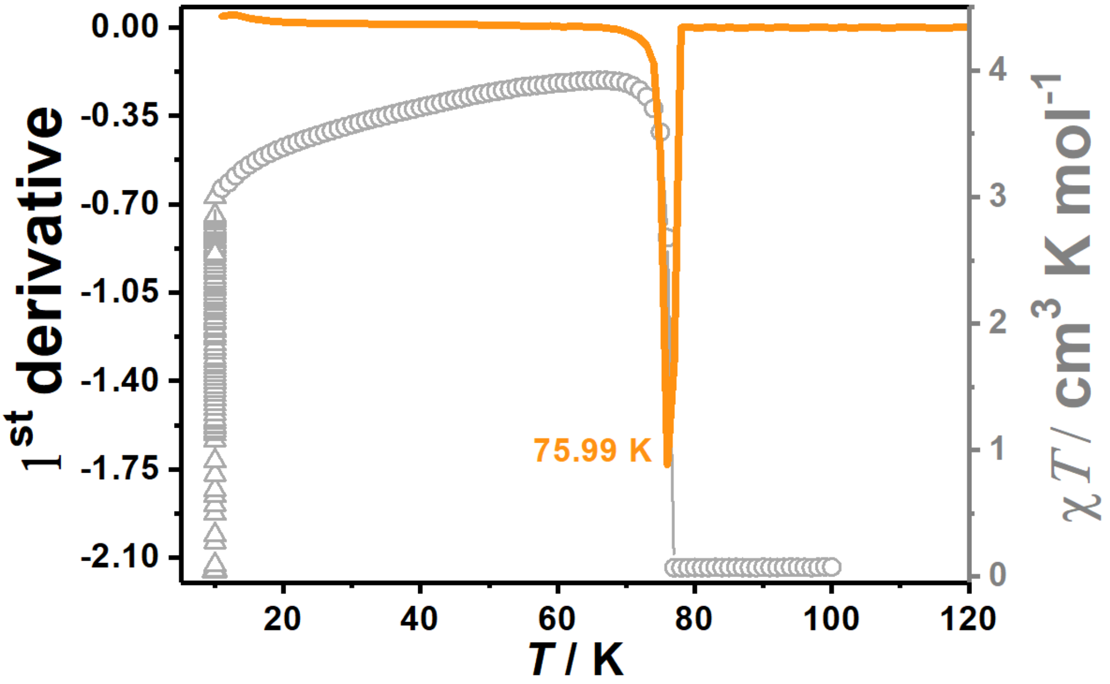

Figure S11. The 1st derivative of photomagnetic susceptibility data.

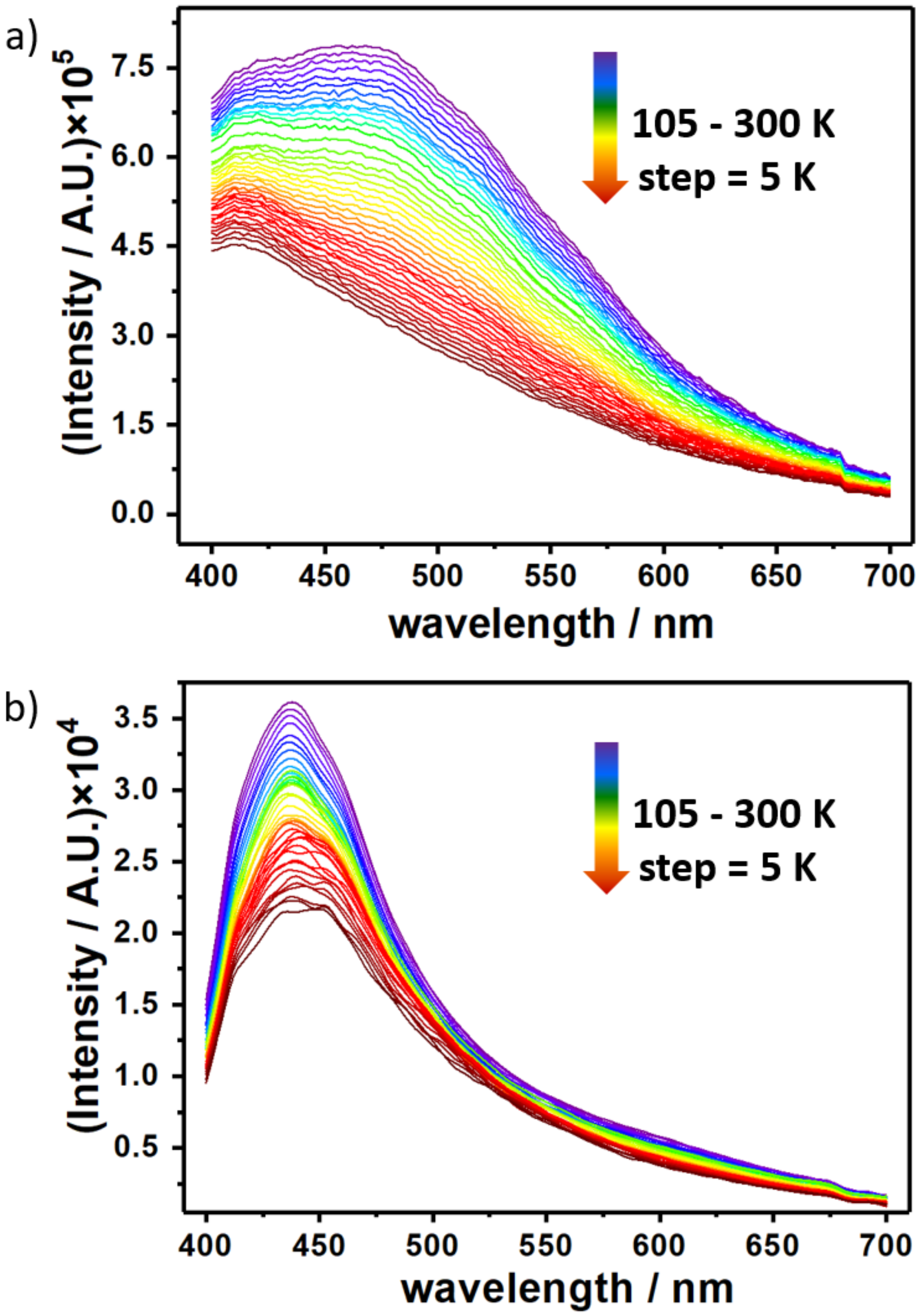

Figure S12. Temperature-dependent fluorescence emission spectra of (a) bis(triphenylphosphine)iminium chloride (PPNCl) and (b) **1** under excitation at 350 nm.

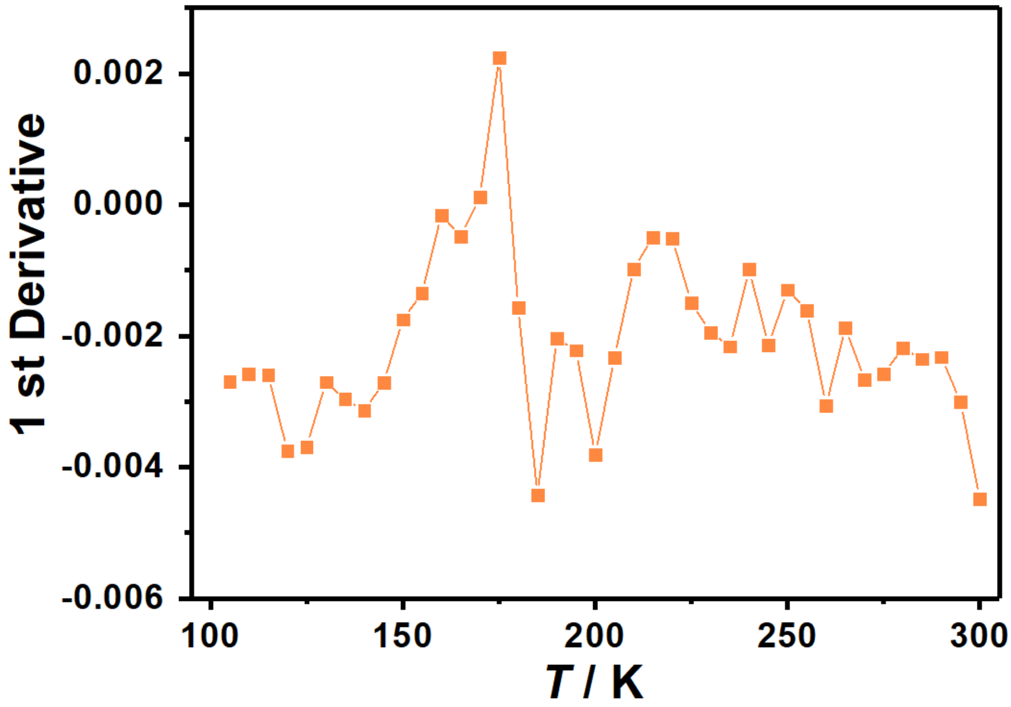

Figure S13. The first derivative plot of temperature-dependent normalized fluorescence emission intensity at 438 nm for **1**.

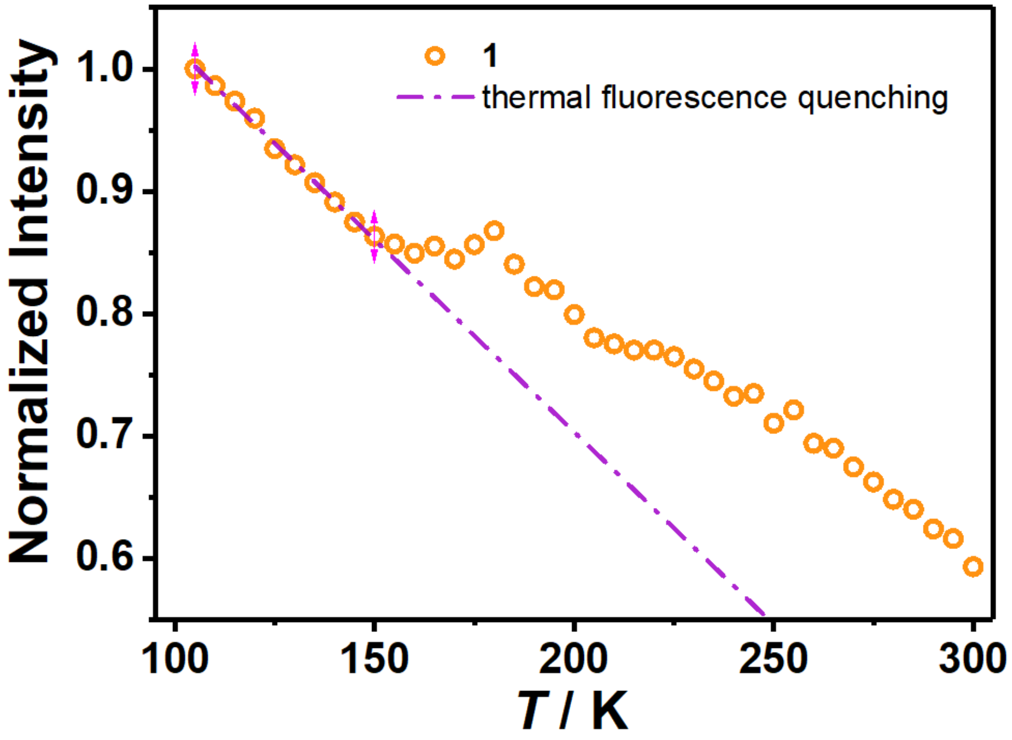

Figure S14. Normalized fluorescence emission intensity at 438 nm as a function of temperature for **1** (orange). The intensity at low temperature region (low-spin state) is linearly fitted to extract the base line of thermal fluorescence quenching (purple dashed line).

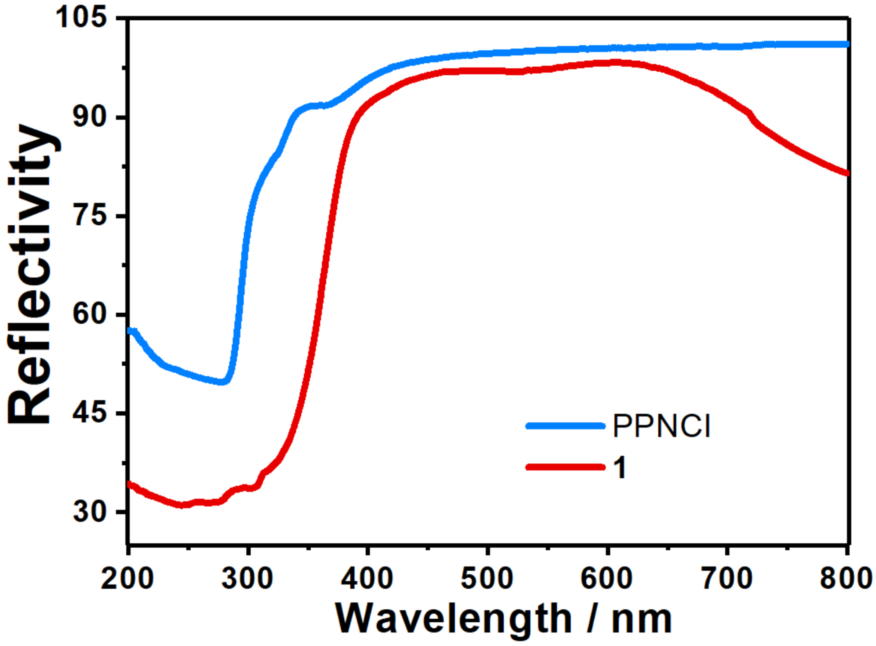

Figure S15. The UV/Vis reflectivity spectroscopy of PPNCl and **1** at room temperature.